HCl Solvation at the Surface and within Methanol Clusters/Nanoparticles II: Evidence for Molecular Wires

Nevin Uras-Aytemiz*

Department of Chemistry, Suleyman Demirel University, 32260 Isparta, Turkey

J. Paul Devlin

Department of Chemistry, Oklahoma State University, 74078 Stillwater, Oklahoma

Joanna Sadlej

Department of Chemistry, University of Warsaw, Pasteura 1, 02-093 Warsaw, Poland

Victoria Buch

The Fritz Haber Institute for Molecular Dynamics, Hebrew University, Jerusalem 1904, Israel

Received: May 5, 2006; In Final Form: August 14, 2006

Condensed-phase solvation of HCl on and within methanol nanoparticles was investigated by Fourier transform infrared (FTIR) spectroscopy, on-the-fly molecular dynamics as implemented in the density functional code Quickstep (which is part of the CP2K package), and ab initio calculations. Adsorption and solvation stages are identified and assigned with the help of calculated infrared spectra obtained from the simulations. The results have been further checked with MP2-level ab initio calculations. The range of acid solvation states extends from the single-coordinated slightly stretched HCl to proton-sharing with Zundel-like methanol $O\cdots H^+\cdots X^-$ states, and finally to $MeOH_2^+\cdots Cl^-$ units with full proton transfer. Furthermore, once the proton moves to methanol, it is mobilized along methanol molecular chains. Since the proton dynamics reflects the evolving local structures, the "proton" spectra display broad bands usually with underlying continua.

1. Introduction

Solvation and ionization of HX (X = Cl or Br) on/in ice have attracted considerable attention as important steps in the depletion of stratospheric ozone.[1,2] Several experimental (see for example refs 3−8) and theoretical (see for example refs 9−12) research groups have questioned whether HCl is molecular or ionic on the surface of ice and, if it ionizes, how efficiently and with what level of H_2O solvation.

HCl solvation on ice nanoparticles at temperatures below 110 K has been studied by us by means of Fourier transform infrared (FTIR) spectroscopy, Monte Carlo simulations, and ab initio calculations on model clusters.[3,4] It was found that solvation and ionization of HCl were dependent on the HCl coverage and the temperature. At low HCl coverage and low temperature, HCl is molecularly adsorbed on ice nanoparticles, forming one or two bonds with the surface: the binding is to dangling-oxygen (d-O) atoms with a second coordination to a dangling hydrogen (d-H) in some cases (i.e., binding to surface oxygen and hydrogen atoms with unused H-bond coordination sites). The corresponding HCl stretch modes for singly and doubly coordinated HCl were assigned to broad bands at 2480 and 1700 cm^{-1}. Recent results from a Quickstep simulation suggest that bound HCl may be fluxional, possibly changing surface coordination on a picosecond time scale.[13] On the basis of past studies by us[4] and others,[5,8,10,12] it appears that hydration-induced ionization of HCl requires a minimum of three hydrogen bonds with water,[9] one to H and two to Cl. The FTIR results indicate that this condition can be achieved by either raising temperature or increasing the surface concentration of HCl. The hydrated contact ion pair, $H_3O^+Cl^-$, then forms. The final step in the surface solvation and ionization of HCl is proton transfer to a shared state between water molecules, the spectroscopic signature of which is the continuous infrared absorption familiar from aqueous acid solutions: the Zundel continuum.[14]

Here we report continuation of research on solvation of HX adsorbed on hydrogen-bonded nanoparticles, with methanol particles selected for a study complementary to that of ice. The aim of this study is to advance molecular-level understanding of acid solvation on a differently H-bonded surface, namely. that of methanol nanoparticles below 110 K in the submonolayer coverage regime. In addition, bonding in mixed acid/methanol nanoparticles is addressed. For this purpose, we combined FTIR spectroscopy of nanoparticles with on-the-fly molecular dynamics and ab initio computational studies of mixed HCl/methanol clusters. Each methanol molecule has only one O−H group, which is used to form hydrogen bonds between methanol molecules.[15] Therefore, lacking d-H sites thought to be necessary for effective acid solvation, the methanol surface was expected to be less conducive to acid ionization than that of ice. (Unlike for ice nanocrystals, there is no d-H band near 3700 cm^{-1} in the FTIR spectra of amorphous methanol nanoparticles.) The preliminary results of this work were published.[16] It has been and will be shown that, contrary to this expectation, extensive ionization is possible following incorporation of some of the

* Corresponding author: e-mail aytemiz@fef.sdu.edu.tr.

10.1021/jp062753z CCC: $33.50
Published on Web 10/10/2006

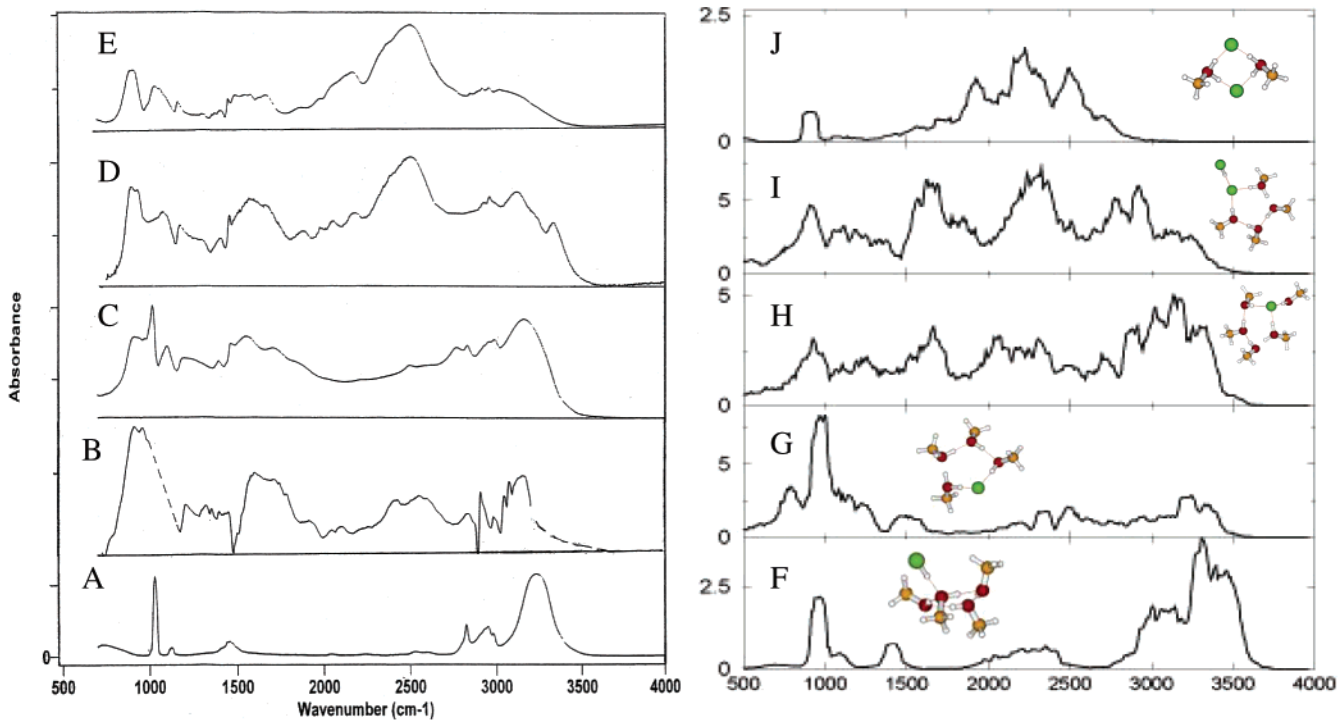

Figure 1. (Left) FTIR spectra of amorphous particles of (A) pure MeOH, (B) lightly dosed HCl on methanol particles at 50 K, (C) HCl/4MeOH, (D) MeOH with "concentrated" surface-adsorbed HCl, and (E) MeOH/HCl. (Right) Calculated spectra from on-the-fly MD simulated trajectories of (F) HCl on $(CH_3OH)_4$, (G) HCl in $(CH_3OH)_4$, (H) (CH_3OH)-(HCl)-$(CH_3OH)_4$, (I) $(HCl)_2$-$(CH_3OH)_4$, and (J) $(HCl)_2$-$(CH_3OH)_2$. The same relative intensity units are used in all calculations; note differences in scale. The inset structures are also shown in Figure 6.

HCl adsorbate in the surface H-bond system, in conjunction with halide solvation by additional acid adsorbate. Moreover, evidence is presented for proton delocalization within the surface. The pertinent measured and computed infrared spectra are shown in Figure 1; note the broad bands and the underlying continua, which are characteristic of proton-transfer systems.

The infrared spectrum of methanol in the solid as well as other phases has been investigated.[15] Size-selected methanol clusters were studied in molecular-beam experiments, with a good review available.[17] Structures, binding energies, and infrared spectra of $(MeOH)_n$, $n = 2-5$ clusters, were calculated by Hagemeister et al.[18] using density functional theory (DFT) methods. Larger methanol clusters, containing 64, 128, 192, 256, and 512 molecules, have been simulated at 200 and 300 K by use of the OPLS potential model to reveal properties of these clusters including the local density and electric potential.[19]

There are few published studies of the HCl-CH_3OH system. The CH_3OH-HCl complex and several of its deuterium isotopomers were studied with microwave spectroscopy.[20,21] Another experimental study, by Fárnik et al.,[22] was based on ragout-jet FTIR cluster spectroscopy. Their spectra included that of the mixed dimer and a trimer of methanol/hydrogen chloride with proposed Cl−H stretch frequencies of 2604 cm^{-1} for the 1:1 complex and 2200 cm^{-1} for the 1:2 complex. Similar study with supersonic jet expansions were combined with ab initio calculations to study cooperative and anticooperative effects of mixed trimers of HCl and methanol.[23] Ab initio computations of mixed dimers and trimers studied with different levels of theory have been reported and structures, energies, and frequencies have been identified in an examination of nonadditive pairwise contributions.[24] The amorphous and crystal methanolates of HX (X = Cl, Br) and CH_3OH were recently identified through their FTIR spectra. Ionic mixed crystals were proposed for CH_3OH:HX ratios of 1:1, 2:1, and 3:1, on the basis of spectral similarity to the corresponding ionic acid hydrates.[25]

The dynamics of proton transfer in liquid methanol was studied by ab initio molecular dynamics at 300 K.[26] Proton displacement was demonstrated along methanol chains, coupled to H-bond strengthening between methanol molecules in the vicinity of the new proton location. The excess proton in methanol clusters was also investigated experimentally. Chang et al.[27,28] reported IR spectra for $H^+(CH_3OH)_n$, $n = 4, 5$, finding that for $n = 4$ the linear structure was the dominant one but for $n = 5$ both linear and cyclic structures coexist at 190 K. With the help of ab initio calculations they also proposed a model for proton motion in the methanol clusters and concluded that the excess proton could be either localized in one methanol unit, $CH_3OH_2^+$, or delocalized between two methanol molecules, $(CH_3OH)_2H^+$. The hydrogen-bond network of larger $H^+(CH_3OH)_n$ clusters, up to $n = 15$, was studied by IR spectroscopy in the O−H-stretch region.[29] The excess proton in ethanol clusters was studied in Ar and N_2 by infrared photodissociation (IRPD) spectroscopy and quantum mechanical calculations. The clusters that have one or three EtOH showed Eigen-type structures, whereas those with two or four EtOH showed Zundel-type structures.[30]

At low temperature (i.e., < 100 K), methanol condenses as an amorphous form with hydrogen bonds linking molecules into chains that are held together by lateral van der Waals forces.[15] The methanol nanoparticles of the present study, prepared near 50 K, were similarly amorphous. Direct many-body simulation of acid-covered methanol particles and of mixed acid/methanol solids is difficult. The main difficulty is inclusion of numerous interacting acid molecules, which may appear in either molecular or ionized state, and concurrent description of all the possible proton states; the latter may include proton localization in methoxonium ions, proton-sharing between two methanol molecules, or proton-sharing between methanol and halide.[25,31] In the present initial computational studies, acid solvation by methanol was investigated with the help of on-the-fly dynamics

and ab initio calculations on mixed acid/methanol clusters. The cluster models correspond to small rings of methanol molecules, with HCl either inserted into the ring or H-bonded externally to one of the ring members. These computational models are of modest size compared to the experimental nanoparticle systems considered. However, condensed methanol and HCl systems tend to be dominated by quasi-linear motifs (chains and rings), and therefore ring clusters may constitute not-unreasonable models. This notion is further supported by the similarity of the experimental and computed spectra in Figure 1.

The main computational tool used in the present investigation is Quickstep, a new-generation on-the-fly code employing DFT in conjunction with Gaussian basis sets.[32,33] Approximations such as reduced dimensionality of the cluster models, DFT, and classical treatment for nuclear molecular dynamics of limited duration are expected to limit the accuracy of the computations to a semiquantitative level. Nevertheless, this technique enables first-principle simulation of both the dynamics and the spectra of these highly anharmonic proton-transfer systems. All the different solvation states can be accessed by this technique, and moreover proton transfer and delocalization can be studied in a time-dependent manner. The corresponding spectra are obtained from the Fourier transform of the dipole−dipole correlation function (Figure 1). The scheme can reproduce broad bands and underlying continua characteristic of the fluxional proton-transfer systems. This is in contrast to the ab initio normal-mode analysis, which assumes small oscillations around a single minimum and produces line spectra. On-the-fly simulations were employed quite successfully to interpret infrared spectra of mixed acid/ether solids[31] and of protonated water clusters.[34]

The left side of Figure 1 shows typical experimental spectra of HCl adsorbed on or solvated within amorphous CH_3OH. Procedures used to obtain these spectra will be described in detail in section 2, but briefly, they are from either HCl-dosed methanol aerosol particles or premixed HCl-CH_3OH amorphous particles. Related calculated spectra are presented in the right side of Figure 1 for different HCl-CH_3OH cluster models used in this study. The computed cluster dynamics is described in section 3. Section 3 includes also the analyses of calculated spectra of the model systems and their relationship to the experimental spectra. The study is summarized in section 4.

2. Experimental Methods and Results

2.1. Experimental Methods. Our FTIR observations of the interaction of HCl and HBr with the surface of amorphous methanol particles were based on three different methods. One method paralleled that used in a previous investigation of the interaction of HX with the surface of ice nanocrystals within a 3D array in the 50−100 K range.[3,4] The particle arrays were generated by pulsing ∼1% mixtures of methanol into a cold condensation cell held near 50 K. A fraction of the cold aerosol particles that form assembles into arrays on the two ZnS infrared windows of the condensation cell. A series of load and pump cycles results in an array of the optimum thickness. To obtain a reasonably uniform doping of HX on the particle surfaces at submonolayer coverage, the methanol particle arrays were assembled near 50 K with alternating embedded layers of much smaller HX nanoparticles. The HX particles complete their evaporation onto the methanol particle surfaces upon warming near 60 K. The acid−particle interaction, as well as the temperature dependence, was followed by monitoring the FTIR spectra over the 50−110 K range. Infrared difference spectra, comparing the acid/methanol samples and pure methanol particles at corresponding temperatures, indicated the impact of the HX adsorbate. Data from a second approach, based on HX dosing of aerosols of methanol nanoparticles within He(g), are also presented. The amorphous methanol nanoparticles were prepared by pulsing a 1% mixture of methanol in He(g) into a double-walled cold condensation cell held near 60 K. The bare particle spectra were then compared with spectra measured shortly after admittance of a second much weaker pulse containing ∼0.2% HX in helium. Finally, the third method was based on exposure of thin 3D arrays of methanol particles to a dilute aerosol of HX nanoparticles in He(g). Each of these methods gave similar spectra for HX interaction with the methanol particle surfaces in the 50−60 K range.

For ice, the extent of the surface doping, that is, the percentage monolayer (ML) of acid coverage of the nanocrystals, was estimated by noting the decrease in intensity of the bands of surface water molecules that accompanies a particular HX dosage.[4,35] This measurement is particularly convenient for the dangling-H surface band near 3693 cm^{-1}. However, the amorphous methanol particles do not have a corresponding band since most O−H groups of the surface molecules readily find neighbor acceptor oxygen atoms with which to bond (see later discussion in section 3). For this reason, the HX dosage level for methanol particles has been estimated as follows: arrays of methanol particles, with O−H band integrated intensities ∼50% of that of the "standard" ice arrays, were prepared from the same solvent/helium mixture concentrations (∼1%) and at the same temperature (50 K). On the basis of the O−H stretch intensity for solid methanol versus ice, this assured a similar amount of methanol, on a molar basis, as the water present within the ice arrays of ref 4. The total surface area of the methanol particles was then estimated from the band intensity of a monolayer of adsorbed CF_4, as described in detail for ice particles[35] (the molecular density of the adsorbed CF_4 is judged from the frequency spacing of the CF_4 asymmetric stretch TO and LO surface modes). This method indicated a total methanol-particle surface area twice that of a corresponding ice array. When adjusted for the relative molar volume of 2.2, this implied an average particle size of ∼12 nm, quite similar to that of the ice samples. However, the greater surface area for the methanol samples signaled ∼50% reduction in acid coverage for the same HX dosage. In this manner, samples with HX surface coverage estimated as ranging from 10% to 50% ML were prepared by the alternating methanol/acid particle approach.

FTIR spectra of the effect of doping methanol particle surfaces with HX in an aerosol phase were obtained via the same cold-condensation cell and similar difference techniques. The methanol aerosols, of particles of ∼12 nm, were first formed at ∼0.3 bar from a pulse of a 1% mixture of HX in He(g) at ∼60 K. Following a brief time delay (∼5 s), a second pulse (of higher stagnation pressure) containing dilute HX in He(g) was admitted to the cell. The resulting difference spectra (comparing bare particles with particles following HCl exposure) presented in Figure 3 are quite similar to those shown for the 3D particle arrays (Figure 2), but it should be recognized that the distribution of the acid throughout the aerosols is not uniform, though it is possible to control the relative HX concentrations from sample to sample. A nonuniform particle dosage is also expected for samples obtained by exposing arrays of methanol particles to aerosols of HX in He(g) since the front layers of an array experience a disproportionate exposure.

The FTIR spectra of amorphous mixtures of methanol/H(D)X with molecular ratios ranging from 6 to 1 have also been determined by two different techniques. The data for HBr and

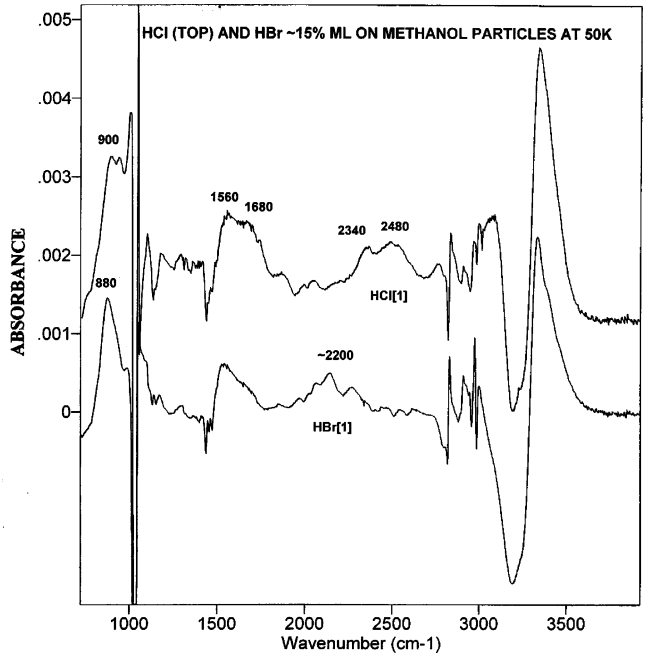

Figure 2. FTIR difference spectra for submonolayer levels of HCl and HBr interacting with the surface of amorphous ~6 nm methanol particles at 50 K. Dosing was by intermixing much smaller HX particles among methanol particles of a 3D array. Subtraction of the spectrum of pure methanol nanoparticles from that of the dosed arrays gives the difference spectra.

HI reported previously,[25] as well as some of the results described below, were obtained from amorphous films formed by cocondensation of HX and methanol vapor beams on a CsI substrate attached to the cold stem of a liquid-nitrogen-cooled infrared cell. New spectra are presented for amorphous particles for a range of methanol/HCl compositions (Figure 5). The particles were prepared by pulsing premixtures of methanol and HCl in He(g), of molar ratios varying from 6 to 1, into a double-walled particle condensation cell held near 70 K. Initially a 5 L vapor mixture of equal molar concentrations was prepared for formation of the amorphous monomethanolate of the acid. Subsequently, methanol/acid mixtures of higher ratios were formed by dilution of the original mixture with methanol vapor within an attached 1-L mixing bulb.

The reagents for the thin films and particles were methanol (Baker Analyzed), HX (Matheson Research Purity >99.8%) and He(g) (Aeroform Corp. Ultrahigh Purity) used after outgassing of the methanol and vacuum distillation of the more volatile impurities from the HX gases.

2.2. Experimental Results. The objective was to prepare and characterize a range of HX solvation states within a methanol environment. The emphasis here is on FTIR spectra of HCl adsorbed (i.e., partially solvated) on amorphous methanol nanoparticles in the 50−100 K range and within amorphous methanol/HCl mixtures prepared by low-temperature vapor codeposition or as cocondensed nanoparticles. Spectra of HBr solvation states within crystalline phases *n*MeOH/*m*HBr ($m = 1$; $n = 1-3$) prepared by annealing the amorphous phase of the appropriate n/m ratio have been published recently,[25] while data for crystalline phases with HCl, for a broader range of relative concentrations ($^1/_3-3$), will appear in a forthcoming paper.

2.2.1. FTIR Spectra for HCl and HBr Adsorbed on Amorphous Methanol Nanoparticles. It is known from recent ice studies[4,5,6] that the nature of the adsorbed state of an acid on an H-bonding substrate can be highly dependent on the temperature, the level of HX surface coverage, and perhaps the phase of the ice.[36] Spectroscopic data for particles[4] and reactive-ion-scattering results for amorphous films[5] both indicate that solvation of isolated adsorbed HX molecules on ice leads to primarily ionized states at temperatures above ~100 K, with molecular states dominant at lower temperatures (though X-ray scattering data for HCl on crystalline ice films have been interpreted quite differently[36]). Further, self-solvation causes the ionic state of HX on ice to be dominant even at 60 K, if the acid concentration exceeds 30% ML.[4] For these reasons, the present study of the interaction of HX with the surface of methanol nanoparticles emphasizes low temperatures (<100 K) and low acid coverage (10−50% ML), to enhance the possibility of observing adsorbed HX states ranging from single H-bonded to more completely solvated and ionized.

2.2.1.1. Acid Adsorbate Effect in Mixed Particle Arrays. The impact of adsorbed HCl and HBr on the FTIR spectra at 50 K, for low acid coverage (10−20% ML from intermixed HX/methanol particle arrays), is compared in Figure 2. These difference spectra (vs bare methanol particles) for the two acids show a high similarity except for the presence of the HCl(1) band at 2480 cm^{-1} and the broader, less well-defined HBr(1) band near 2200 cm^{-1}. As has been noted earlier,[25] broad acid-related bands, such as the HBr(1) band, are often fragmented by antiresonance with superimposed sharp overtone bands of an H-bonding solvent. The labeling of the bands as HX(1) follows symbols used in ref 4, denoting the band of adsorbed molecular HX closest to the gas-phase frequency. For the ice surface, extensive classical and quantum computations firmly associate the HX(1) bands with the presence of a single H-bond to a surface oxygen site. The large (~280 cm^{-1}) offset of this band for HBr versus HCl, as in Figure 2 for methanol particles, has previously been offered as strong evidence of a molecular origin for the HX(1) band of HX adsorbed on ice particles.[4,13]

Particularly intense spectral features in Figure 2, near 1000 and 3250 cm^{-1}, reflect the impact of the adsorbed acids on the most intensely infrared-active vibrational modes of methanol molecules of the surface/subsurface (see methanol particle spectrum of Figure 1). The peak intensities of these bands in the original array spectra were ~0.2 absorbance unit, so the excursions of ~0.005 unit in the difference spectra near 1000 cm^{-1} are consistent with strong involvement of ~3% of all methanol molecules with the HX adsorbate. With ~20% of the methanol molecules at the surface of the 12 nm particles [as calculated from estimated molecular area (0.16 nm^2) and the known molecular volume of methanol], ~15% of the surface molecules appear to be strongly affected by the adsorbates, consistent with an estimate of 15% ML coverage by HX. Because of the intense nature of the bands being subtracted, the difference spectra above 3000 cm^{-1} are somewhat erratic and will be omitted in subsequent figures.

Because of the greater surface area of the methanol particles compared to the ice particles of ref 4, the HX coverage for the same dosage level is lower than for the ice particles. This, together with a near absence of dangling-OH surface groups, would be expected to favor molecular over ionic states of the HX adsorbed on methanol particles. However, consideration of the low-frequency region of the spectra might suggest labeling of bands near 900 and 1600 cm^{-1} to an ionic state resulting from proton transfer from HX to surface methanol molecules. However, the spectrum of the 1:1 ionic MeOH/HBr crystal phase indicates that the methoxonium ion does not have intense bands in this region.[25] In section 3, in light of detailed computational results for small HCl/methanol clusters, the probable origin of

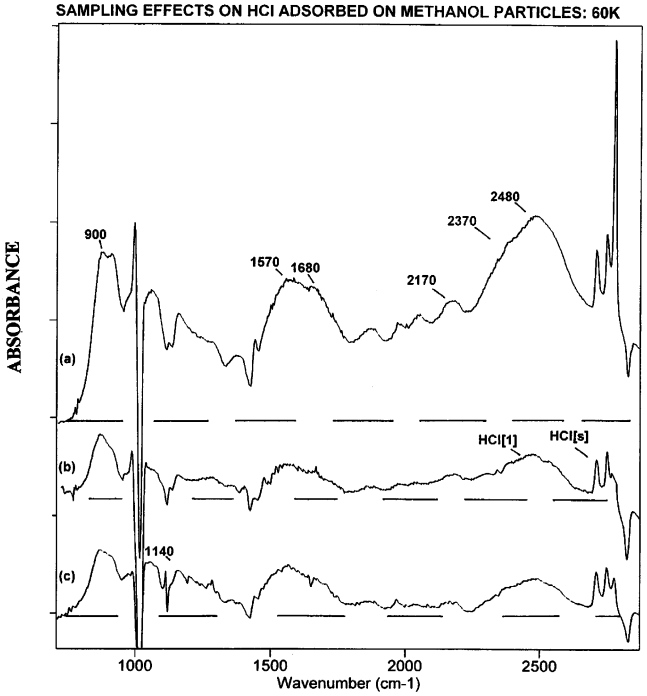

Figure 3. Difference FTIR spectra of HCl adsorbed on the surface of amorphous ~6 nm methanol particles at 60 K. Dosing was by exposure of an aerosol of pure methanol nanoparticles (a, b) and of a thin methanol nanoparticle array (c) to a dilute aerosol of much smaller HCl particles. The acid exposure was greater in (a) than (b) by a factor of 4.

these bands will be related to a degree of proton sharing with surface methanol molecules.

2.2.1.2. HX Adsorbate Effect from Dosing by Aerosol−Aerosol and Aerosol−Array Mixing. A surprising stability of the spectrum of HCl adsorbed on methanol particles near 60 K is addressed in Figure 3. Each of the three samples a−c was prepared under significantly different conditions with respect to each other, and also relative to the top spectrum of Figure 2. Nevertheless, the overall appearance of these difference spectra, obtained by subtraction of an appropriate methanol-particle spectrum, is quite similar. Samples a and b were both prepared by pulsing a dilute mixture of HCl in He(g) into a dense aerosol of methanol particles at 60 K, while the bottom spectrum c is for an array of methanol particles dosed by direct exposure to a dilute aerosol of HCl in He(g) for a few minutes. Thus, sample c was produced by a unique dosing procedure, and a differed from b in that a 4-fold greater volume of HCl−He mixture was pulsed into the methanol aerosol.

Despite the similarity of the spectra (of Figure 3 and the top spectrum of Figure 2), which suggests that HCl adsorbed on methanol particles at low temperatures achieves a similar state under a wide range of sampling conditions, there are subtle differences that offer a basis for a detailed analysis as developed in section 3. For example, the greater HCl dosage for a than b caused the broad absorption intensity in the 2400 cm^{-1} region to increase noticeably relative to that near 900 cm^{-1}. Further, an underlying continuum, typical of shared protons,[4] increased substantially with the increased dosing of sample a. Also noteworthy is the lack of a large relative increase of band intensity at 900, which would be expected for a if that band is caused by ionized HCl. The ionic state of adsorbed HCl on ice particles was shown to be strongly favored by even minor increase in the acid surface coverage, an effect attributed to HCl solvation of the chloride ion, that is, self-solvation.[4]

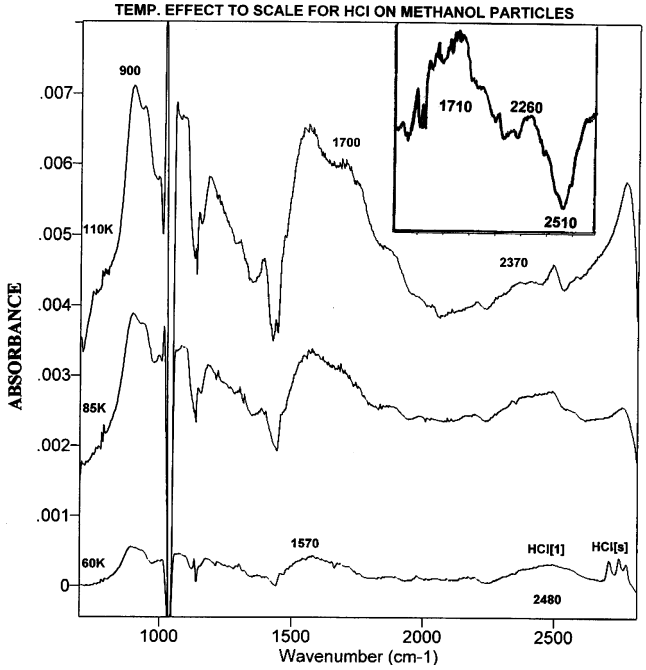

Figure 4. Difference FTIR spectra for the 60 K sample (c) of Figure 3, showing the influence of warming to 85 and 110 K. Spectra are offset for clarity but are on the same absorbance scale. (Inset) Effect, in the 1400−2700 cm^{-1} range, from warming the sample of the top spectrum of Figure 2 from 50 to 70 K. The 50 K spectrum was subtracted from that of the sample at 70 K.

Spectrum c of Figure 3 differs from a and b primarily by the presence of relatively stronger broad-banded intensity in the 1000−1300 cm^{-1} range. Similar banding, as observed in HCl/ether systems, has been related by computations to thorough sharing of a proton,[31] as will also be considered in section 3. Spectrum c otherwise resembles the spectra for the other HCl systems of Figures 2 and 3, that is, characterized by dominant bands at ~900, 1600, and 2500 cm^{-1}.

2.2.1.3. Temperature Response of Adsorbed HCl on Methanol Particles. Though increased acid doping of methanol particles at 50−60 K has less impact on the band pattern of the infrared difference spectra than in the case of ice particles,[4] raising sample temperatures has a pronounced effect similar to that noted for ice. This temperature effect is apparent in Figure 4 for a sample prepared by dosing a methanol 3D particle array with acid by exposure to a dilute aerosol of very small HCl(s) particles. The bottom spectrum, which is the c spectrum of Figure 3 for a freshly dosed 60 K sample, has a "molecular" 2480 cm^{-1} band with an intensity that rivals that of the stronger bands. However, upon warming, to first 85 and then 110 K, all other bands (Figure 3: 900, 1570, 1700, 2370, and the fractured broad band near 1150 cm^{-1}) increase, in concert with the temperature, while the HCl(1) band fades away.

This behavior from warming is greatly amplified for samples with higher levels of acid dosing, for which it is also accompanied by emergence of an intense continuum ranging from 800 to 3000 cm^{-1} (resembling that for ice in Figure 12 of ref 4). This loss of HCl(1) intensity and growth of other bands is similarly observed for sample arrays prepared by alternating the loading of methanol particles with much smaller acid particles. A typical example is given in the inset of Figure 4, where the subtraction of a 50 K spectrum from a 70 K spectrum demonstrates the intensity loss near 2500 cm^{-1} and the associated gains near 2300 and 1700 cm^{-1}.

2.2.2. Infrared Spectra of Amorphous *n*MeOH/HCl Nanoparticles and Thin Films. It has been noted that the spectra of

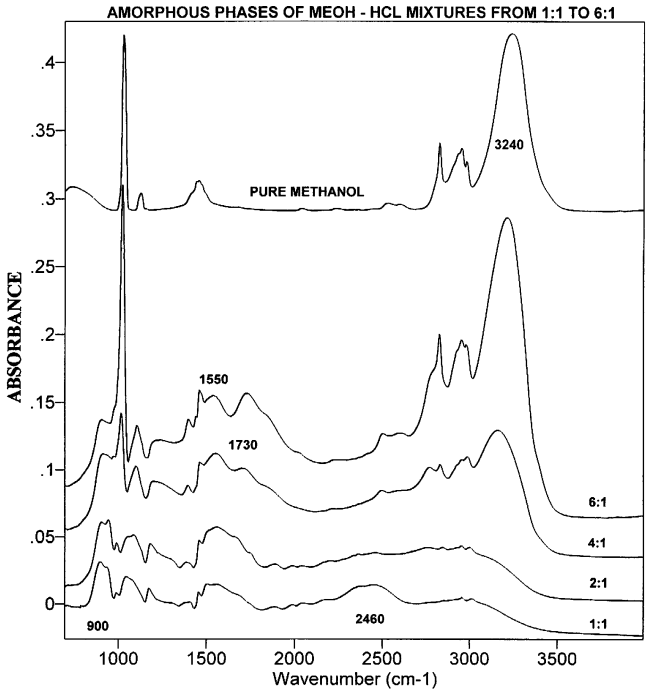

Figure 5. FTIR spectra for aerosols of amorphous nanoparticles of *n*MeOH/HCl for $n = \sim 1$, 2, 4, and 6 at 70 K and of an aerosol of pure methanol nanoparticles. The *n*MeOH/HCl spectra are normalized, roughly, to constant amount of acid. The bottom spectrum corresponds to ~20% more methanol than the top left spectrum in Figure 1.

the disordered structures generated on ice particle surfaces through interaction with HCl and HBr closely resemble the spectra of certain amorphous HX hydrates.[4] This is understandable, since both the surface phase and the bulk amorphous phase are characterized by disorder, localized variations in solvation levels of the acid, and consequently, a range of HX states with varying extent of proton sharing with the solvent. A similar loose analogy might also be expected for HX adsorbed on amorphous-methanol particles and the mixed amorphous solids *n*MeOH/HX. For this reason, it is of interest to compare the adsorbate spectra of Figures 1−4 with spectra for a range of amorphous HX methanolates as given in Figure 5.

The spectra of Figure 5 are for helium aerosols of nanoparticles of *n*MeOH/HCl with $n = 1-6$. Spectra for a narrower range of acid content have been published for thin films of MeOH/HBr (Figure 6 of ref 25). In both instances, there is a clear evolution in the spectra with increasing methanol content. Figure 5 shows that the (molecular) HCl(1) band near 2460 cm^{-1} is strong for the monomethanolate, greatly weakened in the 2:1 mixture, and missing at higher methanol levels. Concurrently, the bands below 1600 cm^{-1} (900, ~1100, and 1550 cm^{-1}) evolve slowly with methanol concentration, while new intense bands, some clearly related to the molecular methanol spectra, become dominant. Perhaps most important to the recognition of associated changes in structure (see section 3) is the emergence of new bands near 1730 (with a shoulder near 1850) and 2550 cm^{-1}. Also particularly noteworthy is the near coincidence between the 1:1 mixed-phase particle spectrum of Figure 5 (below 2700 cm^{-1}) and spectrum a of Figure 3 of a surface state with a high surface population of HCl.

3. Computations

3.1. On-the-Fly Molecular Dynamics Simulations. In these calculations, the electronic structure code Quickstep,[32] which is part of the CP2K package,[33] was employed. Quickstep is an implementation of the recently developed Gaussian plane wave method,[37] which is based on the Kohn−Sham formulation of density functional theory (DFT). The Kohn−Sham orbitals are expanded by use of a linear combination of atom-centered Gaussian-type orbital functions. The electronic charge density was described with an auxiliary basis set of plane waves. Energies and forces from on-the-fly ab initio molecular dynamics simulation sampling of the Born−Oppenheimer surface were calculated for each MD step by use of the atomic pseudopotentials of the Goedecker, Teter, and Hutter type,[37] a Gaussian valence basis set of quadruple-ζ quality augmented by three sets of polarization functions (QZV3P), and the exchange-correlation functional of Becke, Lee, Yang, and Parr (BLYP).[38,39] Each system has been subjected to minimization procedure by using Quickstep before constant-energy MD simulations were performed. Figure 6 presents the clusters, $(HCl)_m(CH_3OH)_n$, $m = 1-2$ and $n = 3-5$, that are used in this study. The time scale for each system will be given in related

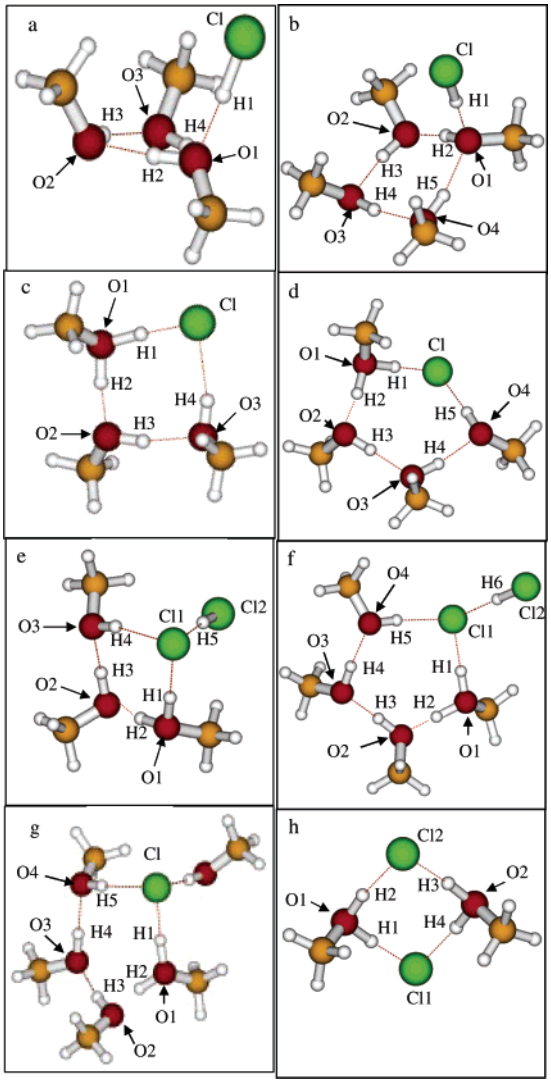

Figure 6. Models used in on-the-fly MD simulations of cluster structures and (proton) dynamics: Quickstep minima. Cluster configurations are referred to in the main text and Supporting Information as follows: (a) HCl-on-$(CH_3OH)_3$, (b) HCl-on-$(CH_3OH)_4$, (c) HCl-in-$(CH_3OH)_3$, (d) HCl-in-$(CH_3OH)_4$, (e) $(HCl)_2$-$(CH_3OH)_3$, (f) $(HCl)_2$-$(CH_3OH)_4$, (g) (CH_3OH)-(HCl)-$(CH_3OH)_4$, and (h) $(HCl)_2$-$(CH_3OH)_2$. The corresponding spectra can be found in Figure 1: spectrum F for model b, spectrum G for model d, spectrum H for model g, spectrum I for model f, and spectrum J for model h.

result part. The cluster spectra were obtained from the Fourier transform of the dipole−dipole correlation function.

3.2. Details of Ab Initio Calculations. Ab initio calculations on the cluster structures are shown in Figure 6a−e. B3LYP- and MP2-level calculations included energy minimizations and normal-mode analysis. The objective was to calculate HCl bond lengths and frequencies for minima associated with different coordinations/structures, rather than to necessarily locate the global cluster minimum for a given cluster composition.

The B3LYP and MP2 calculations were carried out with Gaussian 98.[40] MP2 method was included in addition to the commonly employed and cheaper B3LYP, since the latter sometimes overestimates the tendency of solvated HCl to stretch and ionize. [This conclusion was reached from earlier comparison of MP2 and DFT results in the aug-cc-pVDZ basis set and is in accord with past comparative studies employing MP2 and B3LYP with larger basis sets for $(H_2O)_n\cdots(HCl)$ clusters.[4,41,42]] Full geometry optimizations were performed with the most stringent internal criteria (very tight option) at B3LYP and MP2 frozen-core level. Harmonic frequencies and infrared intensities were calculated by use of analytical second derivatives. The aug-cc-pVDZ basis set was employed in the calculations. This basis set is the largest that could be realistically used with our computer resources for optimization and frequency calculations at a correlated level, for the largest cluster sizes. The same basis set was retained for smaller clusters as well, to obtain trends as a function of size on a consistent level of accuracy. As shown in ref 43, it reproduces rather well the geometries, frequencies, and electric properties of hydrogen-bonded clusters. The MP2/aug-cc-pVDZ HCl bond length and fundamental harmonic frequency were calculated as 1.2879 Å and 3023 cm^{-1}, as compared to experimental values of 1.275 Å, and 2991 cm^{-1}, respectively.[44] For CH_3OH, the OH and CO bond lengths and OH, CO fundamental frequencies were calculated at the MP2/aug-cc-pVDZ level as 0.9657 and 1.4345 Å and 3842 and 1045 cm^{-1}, as compared to experimental values of 0.981 and 1.417 Å[45] and 3681.5 and 1033.5 cm^{-1}.[15]

The ab initio calculations were used primarily to double-check on-the-fly simulation results and are therefore included in the following discussion of the on-the-fly trajectories. The different ab initio calculations for different structures are summarized fully in the Supporting Information.

3.3. On-the-Fly Dynamics of Mixed Acid/Methanol Clusters: Computational Results and Discussion. A number of $(HCl)_n(CH_3OH)_m$ ($n = 1-2$, $m = 1-5$) trajectory calculations were carried out with on-the-fly molecular dynamics, as described below.

3.3.1. HCl-on-$(CH_3OH)_3$ and HCl-on-$(CH_3OH)_4$ Clusters. The structures are shown in Figure 6a,b. These structures constitute a minimalistic model for HCl adsorbed on the methanol nanoparticle surface at sufficiently low temperature that the acid does not break into the surface hydrogen-bond network. Admittedly, the model "nanoparticle" includes a single ring of only three or four methanol molecules. However, condensed methanol is known to be dominated by chains and rings of two-coordinated molecules,[15,26] so the present model may be a not-unreasonable representation of a portion of the nanoparticle system. This notion is supported by the excellent agreement between the measured pure methanol nanoparticle spectrum, and the computed cluster spectrum (see Figure 1A,F), with the exception of the computed 2400 cm^{-1} band, which originates from the adsorbed HCl. In the two cluster models, there is no free hydrogen of methanol and the methyl groups of methanol are not active sites for strong bonding. Therefore, the HCl molecule acts as a proton donor bonded to single oxygen but aligned perpendicularly to the plane of the ring formed by three (or four) oxygen atoms of the methanol molecules.

Since both structures show similar trends, here only results for the larger cluster are explained in detail. The trajectory was run for 4 ps at an average temperature of 108 K. During the MD run, the average H−Cl bond length was 1.3421 Å with standard deviation (SD) = 0.1396 and the corresponding HCl-stretch mode band is near 2250 cm^{-1}, somewhat below the experimentally observed low-temperature band[1] of the HCl adsorbate at ∼2400 cm^{-1} (see Figures 1−3). The corresponding normal-mode HCl frequency obtained from ab initio calculations was 2310 cm^{-1} (B3LYP) or 2193 cm^{-1} (MP2). A similar peak frequency for singly coordinated HCl, labeled HCl,[1] was proposed for HCl on the ice surface.[3,4] For cluster b, the average OH bond length was 1.0089 Å (with SD = 0.1253) for O1H2, 0.9978 Å (SD = 0.1208) for O2H3, 0.9920 Å (SD = 0.1208) O3H4, and 0.09869 Å (SD = 0.12) for O4H5 (the atom labels are in accord with Figure 6b). The corresponding frequencies, calculated from Fourier transform of the O−H-bond trajectories, are 3150, 3310, 3420, and 3510 cm^{-1}, respectively. A similar trend for O−H bond lengths and frequencies is found for MP2-level calculations (see Supporting Information).

3.3.2. HCl-in-$(CH_3OH)_3$ and HCl-in-$(CH_3OH)_4$ Ring Clusters. The optimized structures are given in Figure 6c,d. In these two structures HCl is incorporated in the methanol ring. The corresponding two-coordinated acid configuration may be representative of a product of insertion of HCl adsorbate into methanol chains within the nanoparticle surface. For c and d clusters, the trajectories were run for 4 and 3 ps, at average temperatures of 98 and 93 K, respectively. Since the two cluster trajectories gave very similar results, only the larger one is examined here. The time evolution of HCl and OH bond lengths, and the corresponding frequencies from their Fourier transforms, are given in Figure 7. It is seen that the acid proton undergoes large amplitude fluctuations between O1 and Cl. The average bond lengths are 1.6081 Å (SD = 0.3036) for H1Cl and 1.2114 Å (SD = 0.2891) for O1H1. One may ask whether these results correspond to proton transfer to O1 or proton sharing between O1 and Cl (the larger size of Cl with respect to O should be taken into consideration). The "proton sharing" description seems more appropriate, because of the large amplitude fluctuations of the proton between O1 and Cl (Figure 7, two left bottom panels) and the mean O1H1 bond length, which is ∼15% or more that of methoxonium (as described further below). This proton-sharing interpretation is supported by the low ∼1000 cm^{-1} peak frequency of the O1H1 vibration.

The remaining OH bonds become shorter as their distance from the proton, counterclockwise along the methanol chain, increases. Thus the average bond lengths are 1.0505 Å (SD = 0.1717) for O1H2, 1.0118 Å (SD = 0.1138) for O2H3, 1.0024 Å (SD = 0.1172) for O3H4, and 0.9941 Å (SD = 0.1095) for O4H5. The bond frequencies are blue-shifted accordingly. It is interesting to note the relative weakness of the H5Cl hydrogen bond on the other side of the chloride, as reflected by the relatively short O4H5 distance. It appears that presence of a very strong hydrogen bond of Cl^- to the protonated methanol on one side weakens the hydrogen bond to methanol on the other side.

The computed infrared absorption spectrum (Figure 1G) is dominated by the intense proton sharing feature at ∼1000 cm^{-1}. Some of the intensity originates from the methanol C−O stretch, which is, however, amplified significantly by the interaction

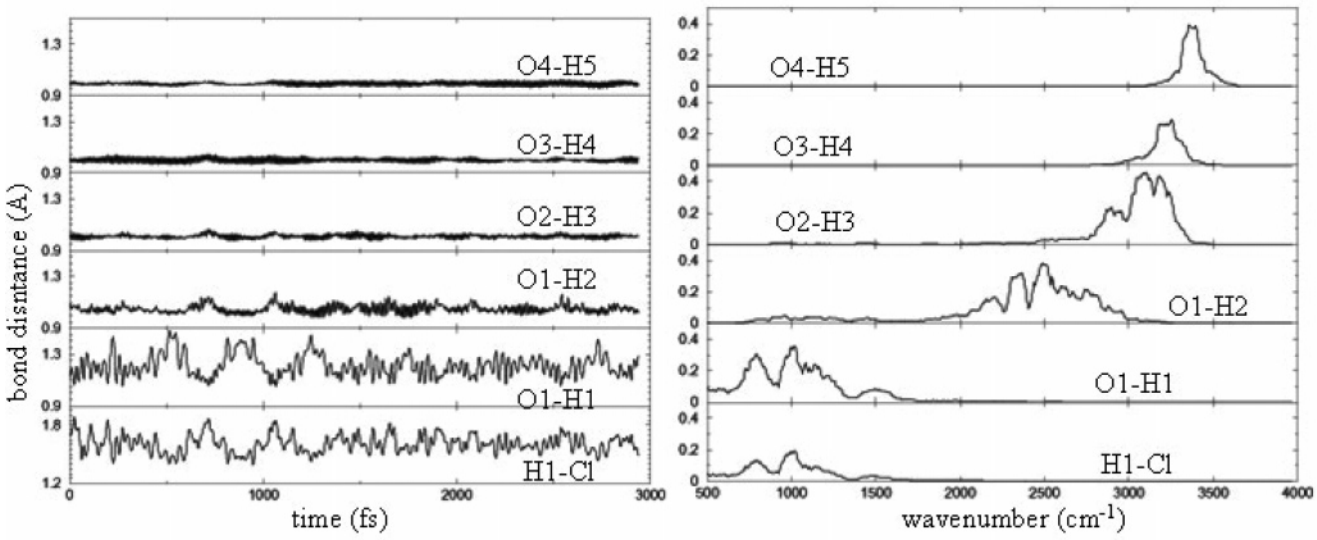

Figure 7. Time evolution of HCl and OH bond lengths (left) and the corresponding frequencies from Fourier transformation of bond lengths for the HCl-in-$(CH_3OH)_4$ case (right) during a 3 ps run at an average temperature of 93 K.

with the proton; note the difference in scale between panels F and G in Figure 1. A similar prominent feature at ~1000 cm^{-1} is observed in surface spectra of methanol nanoparticles exposed to low coverage of HCl (Figure 1B). One can envisage some of the adsorbate molecules breaking into the methanol chains and rings within the surface and adopting a two-coordinated proton-sharing configuration. One may note at this point that we in fact observed such "break-in" in an extended on-the-fly trajectory starting from configuration a in Figure 6 (with HCl adsorbed on a three-membered ring) and ending with a four-membered ring c, in which HCl is a part of the ring. We did not succeed to observe a similar trajectory connecting configuration b of Figure 6 (HCl adsorbed on a larger four-membered methanol ring) with configuration d, on a computationally feasible time scale (~20 ps). However, at the present level of Quickstep calculation, the minimum energy of structure d is lower by ~600 cm^{-1} (~1.8 kcal/mol) than that of b. [A very similar energy difference (1.83 kcal/mol) between structures b and d was obtained in a B3LYP electronic structure calculation, while the value of 1.729 kcal/mol was obtained in MP2.] Thus, relaxation from a singly coordinated adsorbate configuration to a two-coordinated configuration with HCl incorporated in the methanol rings or chains makes sense.

One may note at this point a significant discrepancy between the frequency of the shared-proton band obtained in on-the-fly dynamics at ~1000 cm^{-1} and the corresponding normal-mode frequency obtained in a B3LYP calculation (1323 cm^{-1}). The large discrepancy is not too surprising considering the anharmonic nature of the pertinent motion.

3.3.3. Proton Wire Clusters $(HCl)_2$-$(CH_3OH)_3$, $(HCl)_2$-$(CH_3OH)_4$, and (CH_3OH)-(HCl)-$(CH_3OH)_4$: Dynamics of a Delocalized Proton. In these clusters, extra acid solvation is provided by an additional hydrogen bond to HCl. In the first two clusters, the additional solvation is provided by connecting a second "adsorbate" HCl to the chloride in the ring structures (c and d) described above. The resulting optimized structures are shown in Figure 6e,f. It is seen that additional solvation results in completion of proton transfer from the acid to the neighboring methanol, yielding an ion pair. The two models (e and f) constitute a crude representation of a nanoparticle surface at high acid coverage, at which some HCl was incorporated in the methanol H-bond system, while the remaining singly coordinated HCl provides additional solvation to the incorporated acid. In model g, the third H-bond to the acid is provided by an additional methanol molecule rather than by HCl; again, the third bond is sufficient to induce complete ionization. The latter type of three-coordinated configurations is expected to be present inside methanol-rich mixed acid/methanol solids. The ionization of triply coordinated HCl was observed in the past for the water solvent, in electronic structure studies of mixed HCl/water clusters by others[9,46] and by ourselves.[3,4] On-the-fly study enables investigation of cluster dynamics in addition to minima. The dynamics turns out to be rather striking. The proton hops all around the ring, on the time scale of only a few picoseconds (Figures 8 and 9). This freedom of motion is likely to be characteristic of condensed-phase methanol-containing systems to a much more significant extent than of water-containing ones. This is since water tends to form three-dimensional H-bond networks, with two donor and two acceptor bonds on each H_2O. Proton transfer along one of the acceptor bonds was shown to be impeded by the second acceptor bond.[4,47,48] Thus transfer would occur along paths where the second acceptor bond is absent. Or the activation energy may be required to eliminate it. On the other hand, the two-coordinated chain and ring structures are retained in condensed-methanol systems, similarly to the present cluster models, since a methanol molecule does not form commonly a second acceptor bond even in condensed phases.[26] Thus, one can reasonably expect acid proton delocalization along portions of the chains within the methanol-containing solids. This point is further addressed below in the context of a comparison between the measured nanoparticle spectra and the calculated cluster spectra.

Snapshots from a 4 ps trajectory of cluster f run at 104 K average temperature are shown in Figure 8, with the time evolution of each OH bond distance given in Figure 9. The initial structure is marked "beginning" in Figure 8, with oxygen and hydrogen atoms labeled in order to follow the trajectory of the proton. The hydrogen atom labeled as H1 comes from the HCl2 molecule, which ionizes as the additional solvation of chloride by HCl1 promotes completion of the proton transfer to a neighboring methanol molecule. Let us compare now this case with the (HCl)-in-$(CH_3OH)_4$ cluster case shown in Figure 6d. The major difference is the "adsorbed" HCl molecule, which solvates and stabilizes Cl^- so that it can easily transfer a proton to methanol. Subsequently, the proton moves along the methanol chain.

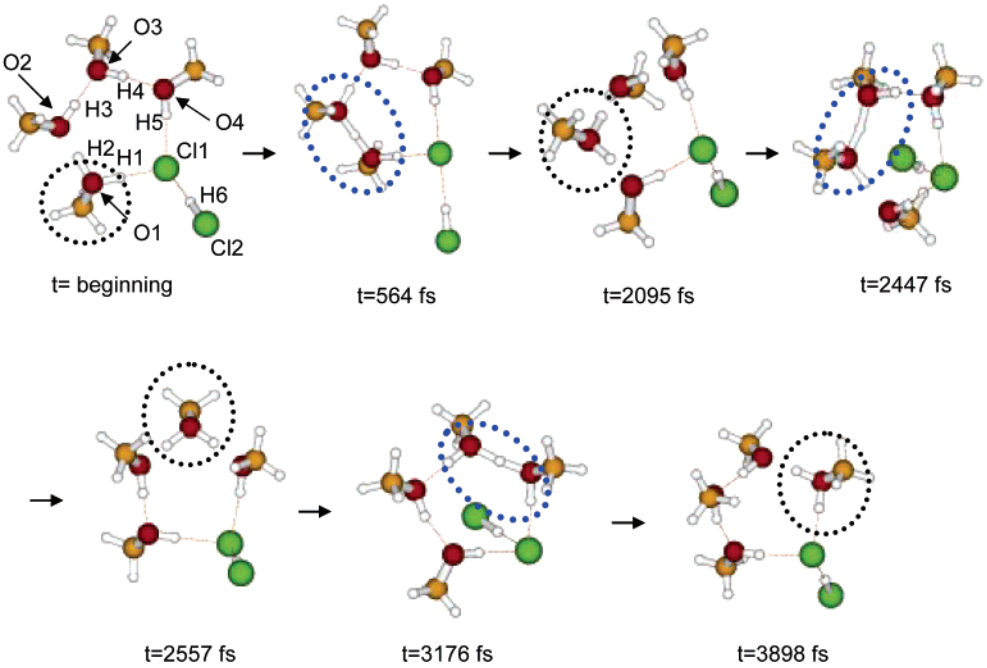

Figure 8. Snapshots of the dynamics of the system $(HCl)_2$-$(CH_3OH)_4$ at various times. Black dotted circles show methoxonium ($CH_3OH_2^+$), and blue dotted circles indicate the proton shared state (i.e., $CH_3OH\cdots H^+\cdots CH_3OH$).

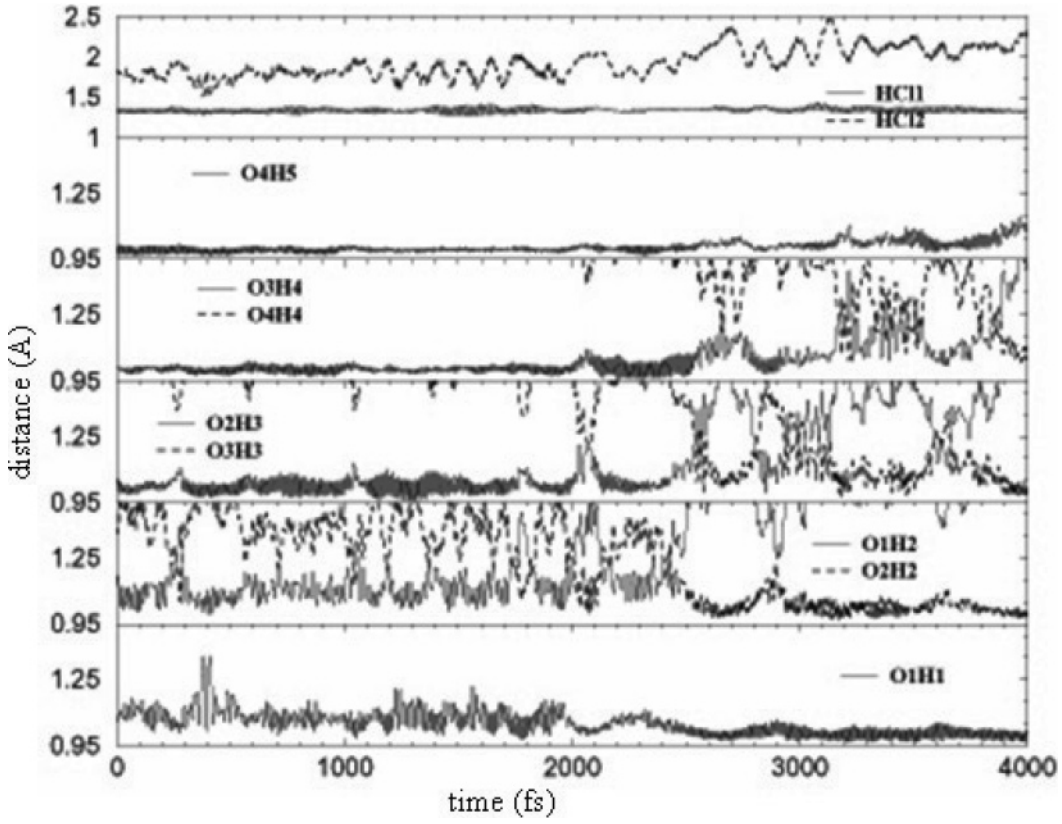

Figure 9. Time evolution of the O−H bond lengths for the $(HCl)_2$-$(CH_3OH)_4$ cluster. The atom labels are shown in Figure 6c.

The proton does not always move forward (i.e., clockwise) but jumps back and forth with formation of transient states, such as a proton-sharing species $CH_3OH\cdots H^+\cdots CH_3OH$ (e.g., see the 564 fs snapshot) as well as $Cl^-\cdots H^+\cdots CH_3OH$ (if the proton is between HCl and CH_3OH; not shown). The proton spends most of the time in a localized methoxonium form $CH_3OH_2^+$ (such as the 2447 fs configuration); first, for about 2000 fs, at the O1 position; afterward, for a few hundred femtoseconds, at the O2 position; and then, for more than 1000 fs, at the O3 position. Proton transfer to O4 occurs at the very end of this trajectory. Cl^- blocks further proton passage in the clockwise direction. While the dominant protonated species observed during the trajectory was $CH_3OH_2^+$, methoxonium OH bonds undergo occasional excursions toward proton-sharing configurations with a neighbor, which sometimes result in proton transfer. The transient proton-sharing species had short lifetimes of ≤ 0.1 ps; however, the corresponding infrared intensity is so large that a band at ~ 1000 cm^{-1} is obtained in the calculated spectrum

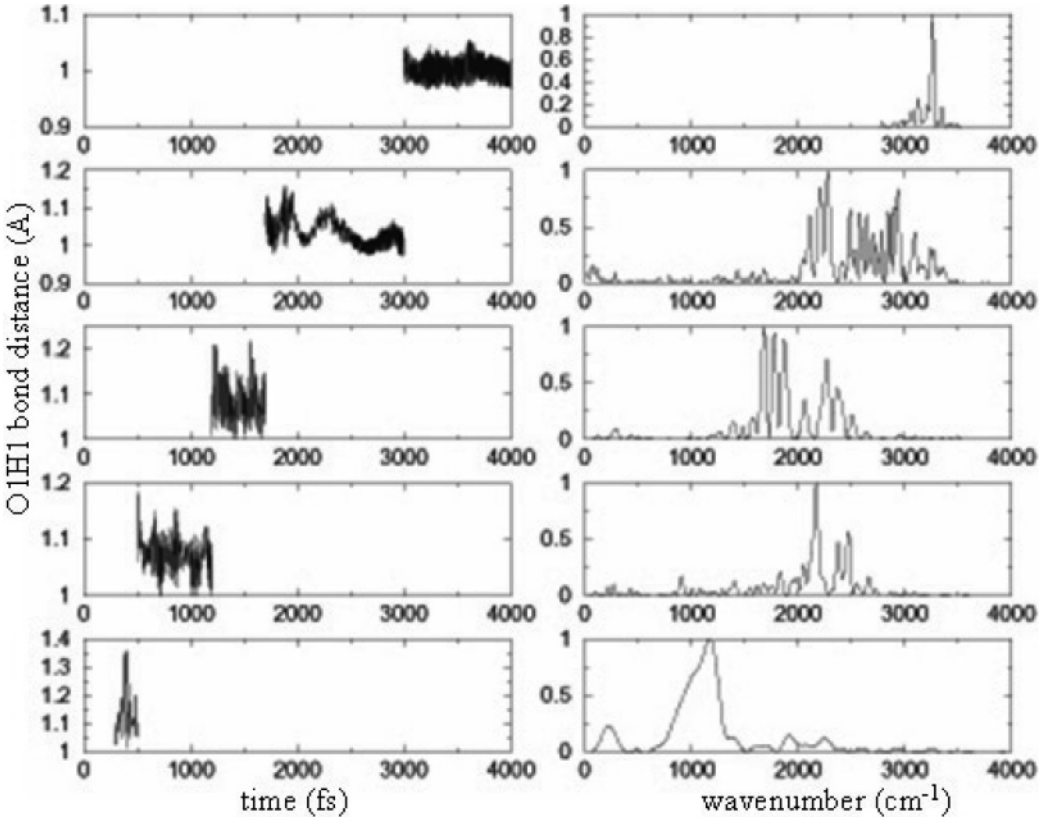

Figure 10. (Left) Time evolution of the O1−H1 bond distance: each row shows a different time period from the given trajectory. (Right) Spectra of each segment from Fourier transformation of corresponding portions of the trajectory.

in Figure 1I. The broad bands at 1640 and 2300 cm^{-1} are assigned to asymmetric and symmetric OH-stretch of methoxonium; the high-frequency part of the second band has an additional contribution from the solvating molecular HCl. The high-frequency end of the spectrum is dominated by the methanol OH stretch. The above assignment was made on the basis of the Fourier transform of trajectories of the appropriate coordinates. One may compare the above frequency values to the ones obtained from normal-mode analysis of structure f in Figure 6, employing B3LYP. Two nearly isoenergetic minima were found for this configuration, corresponding to two different relative arrangements of methanol moieties. The corresponding asymmetric methoxonium stretch frequencies were 1597 and 1817 cm^{-1}, respectively. For both minima, a pair of higher frequency intense infrared bands was obtained, at 2286 and 2493 cm^{-1} and at 2252 and 2440 cm^{-1}, for two normal modes that include both symmetric methoxonium stretch and solvent HCl stretch components (see Supporting Information). These results are qualitatively consistent with the assignments made on the basis of on-the-fly trajectories. (Note that the structures used in the normal-mode analysis correspond to only one of the two physically distinct locations of methoxonium; in the second the proton is localized on O2.)

In on-the-fly trajectories, "proton" mode response to local structural fluctuations strongly influences the spectrum, as can be illustrated for a single O−H bond. The left panels of Figure 10 show the time evolution of the O1H1 bond distance and right panels show the computed spectra from the Fourier transform of each trajectory segment. The first segment, from 0.3 to 0.6 ps, corresponds to the $Cl^{-}\cdots H^{+}\cdots O$ proton-shared structure. As one can see from the corresponding spectrum, this gives a broad band near 1000 cm^{-1}. The following two segments, from 0.6 to 1.2 ps and from 1.2 to 1.7 ps, correspond to proton localization on O1, as methoxonium. In 1.7−3.0 ps segment, the proton moved away, but O1H1 vibration is still perturbed by its vicinity. The last segment (3.0−4.0 ps) for this O1H1 bond reflects a more-or-less "normal" methanol O−H bond with absorption peaked near 3350 cm^{-1}. The total superimposed spectral width of this single OH bond would be very large, extending from 1000 to 3350 cm^{-1}, in accord with the large width of the infrared absorption spectrum calculated from the cluster dipole−dipole correlation function (Figure 1I).

In addition to four broad features assigned above, the cluster spectrum includes an underlying continuum that most likely reflects the fluxional nature of the proton. This calculated spectrum (Figure 1I is in reasonable agreement with that of methanol nanoparticle surface exposed to a high coverage of HCl (Figure 1D), which also includes four broad features and an intense underlying continuum. It is then suggested that at high coverage some of the adsorbed acid molecules break into the surface H-bond network, contributing mobile protons, while the remaining HCl solvate the chloride ions, thereby facilitating this proton mobility. Similar intense continua, observed in the IR spectra of acid solutions in water,[14] were assigned to fluxional protons whose motion reflects a continuous interconversion between $H_5O_2^{+}$ and H_3O^{+} protonated water species.[14,34] However, proton transfer reported for water clusters differs with respect to the present models because of the multiple paths offered by chain branching.[29]

In the course of the trajectory, the proton moves along the entire methanol chain, with much retracing of its steps. It cannot cross the chloride ion, but it can move backward and return to the original position, given a sufficiently lengthy trajectory. The resulting spectrum differs from that of cluster f by reduced intensity in the 2000−2500 cm^{-1} range, where solvating HCl contributed in cluster f, and enhanced intensity in the high-frequency end, originating from the additional (chloride-solvating) methanol molecule; compare spectra H and I in Figure

1. The spectrum of cluster g is in reasonable agreement with that of the 1:4 mixed amorphous acid/methanol solid (see spectra C and H in Figure 1). The underlying continuum in the measured spectrum suggests significant proton delocalization within the solid, along portions of methanol chains. The measured spectrum appears to have enhanced intensity in the $\sim$1000 cm^{-1} region, with respect to the calculated one of cluster g, suggesting that the solid includes three-coordinated ionized acid, as in cluster g, along with some two-coordinated proton-sharing, as in cluster d.

One potential source of worry, concerning the present results on proton-wire clusters, is a possibility of inadequate representation of the relative energetics of the minima and the barriers in the cluster, on the present level of the Quickstep calculation (BLYP/QZV3P). A limited ab initio checkup was made on the smallest cluster model that displays proton delocalization in on-the-fly dynamics: namely, structure e of Figure 6. In the course of the trajectory, the proton visited O1, O2, and O3 positions; however, the first and the last are physically equivalent. B3LYP and MP2 minimizations were carried out for the first and second proton positions, together with the intervening transition state. The energy difference found between the second and first minima was 220 cm^{-1} (B3LYP) or 110 cm^{-1} (MP2). The transition-state energy was only $\sim$20 cm^{-1} (B3LYP) above the higher minimum. These results are consistent with the facile proton transfer along the wire.

3.3.4. $(HCl)_2$-$(CH_3OH)_2$ Cluster. This cluster corresponds to the alternating acid-methanol-acid-methanol pattern. The Quickstep optimized structure shown in Figure 6h contains ionized HCl only; this result was confirmed by MP2. While the acid is only two-coordinated, ionization appears to be induced by a cooperative effect of the kind that is commonly observed in mixed solids. For example, HCl/water dimer is molecular and contains a normal hydrogen bond, while the 1:1 HCl/water solid is fully ionic and composed of halide and hydronium ions;[49] the ionization is induced by mutual solvation of the components. However the four-membered ring cluster HCl-water-HCl-water was shown to be molecular in both MP2 and DFT calculations,[4,46] albeit with ionic minimum only slightly higher in energy. Also, in contrast to the water case, the $(HCl)_2$-$(NH_3)_2$ cluster was found to be ionic.[46] This is understandable since the proton affinity of ammonia is higher than that of water (as is that of methanol to a much lesser degree).

For a cluster h trajectory run of 4 ps at an average temperature of 70 K, the average HCl bond lengths were 1.8280 Å (with SD = 0.3162), with average OH bonds of $\sim$1.077 Å (SD = 0.1732). The corresponding spectrum obtained from Fourier transform of the dipole−dipole correlation function is shown in Figure 1J. The calculated spectrum is similar to the experimental 1:1 HCl/methanol nanoparticle spectrum of Figure 1E, suggesting that this amorphous solid is ionic and composed of chloride and methoxonium ions. Extra intensity in the low-frequency regime of the experimental spectrum suggests, however, some presence of a Zundel analogue, with proton sharing either between two methanol molecules or between methanol and chloride.

4. Summary

Solvation of HCl by methanol in solid systems has been investigated by FTIR spectroscopy of acid adsorbate/methanol nanoparticle systems and of mixed acid/methanol amorphous nanoparticles. In parallel, on-the-fly dynamics and ab initio studies were carried out of mixed acid/methanol clusters shown in Figure 6. The basic structural unit of the model clusters was a ring of methanol molecules, with HCl either inserted into the ring or adsorbed onto the ring. These models are used as a "zero-order" representation of small portions of the experimental condensed-phase systems, since condensed methanol tends to be dominated by molecular chains and rings.[26] Similar studies were carried out in the past on the HCl/H_2O systems (with the help of FTIR, ab initio) and HCl/ether systems (FTIR, on-the-fly dynamics, ab initio).[3,4,31]

In contrast to the ice surface, which offers both dangling-O and dangling-H sites to the acid adsorbate molecules, methanol surfaces include only dangling-O sites. This is because H-atoms of the methanol OH-bond are involved in bonding between surface molecules. At low temperatures and coverages, HCl adsorbate is attached via a single H-bond to the dangling-O sites. Presence of such singly coordinated slightly perturbed molecular acid is evidenced by an experimental band HCl^1 at $\sim$2480 cm^{-1} (Figures 1−3), which is weakened upon heating. A similar band was calculated in clusters for HCl adsorbed on a methanol ring. The HCl^1 band was identified experimentally in the past at $\sim$2480 cm^{-1} for HCl adsorbate on ice.[3,4]

A lower energy two-coordinated acid configuration can be accessed by an activated "break-in" of the adsorbate into methanol chains within the surface. Calculations on ring clusters, with HCl incorporated into the methanol ring (Figure 6c,d), show that doubly coordinated acid displays proton sharing with the neighboring methanol molecule. The corresponding spectral feature, an intense band at $\sim$1000 cm^{-1}, has an experimental counterpart in the nanoparticle surface spectrum at low acid coverage (Figure 1B,G). It appears that, even at 50 K, some of the acid adsorbate molecules manage to break into the H-bonded chains of methanol within the surface. The corresponding two-coordinated HCl band was identified at $\sim$1700 cm^{-1} on the ice surface, originating from a strongly perturbed but still molecular state;[4] the difference with respect to the methanol particles is most likely due to (a) methanol being a better proton acceptor and/or (b) in the absence of surface dangling O−H groups, the methanol surface provides the HCl no competing low-energy two-coordinated sites.

A third hydrogen bond to the Cl side of acid induces completion of the proton transfer, to form a methoxonium and chloride ion pair. This effect was demonstrated computationally by attaching an additional HCl "adsorbate" molecule to the Cl end of the HCl incorporated in the ring cluster (Figure 6e,f). Attachment of an additional methanol molecule instead of HCl has a similar effect. The requirement for three H-bonds to induce acid ionization was similarly reported in the past for the HCl/H_2O systems.[4,9]

The use of on-the-fly dynamics enables the following of the proton dynamics beyond the initial formation of the ion pair. It is shown that the proton hops around the ring cluster, forming methoxonium ions at the different ring sites, on the time scale of only several picoseconds (Figure 8). The calculated spectra reflect the proton dynamics and include a broad symmetric/asymmetric stretch doublet of the methoxonium at 1640 and 2300 cm^{-1} and a feature at $\sim$1000 cm^{-1} from transient proton-sharing states. The underlying continuum most likely reflects the fluxional proton dynamics. Note the large infrared absorption intensity of the fluxional system, as compared to the nonionized one (i.e., compare scales of Figure 1 panels F and I).

The spectrum of the fluxional ring cluster with inserted HCl and extra-solvating HCl adsorbate (Figure 6f) is in qualitative agreement with the measured spectrum of the methanol nanoparticle surface at high acid coverage (compare Figure 1 panels

D and I). It is then suggested, for the experimental system, that some of the adsorbate is incorporated into methanol H-bond chains within the nanoparticle surface, while the remaining acid provides additional solvation of the incorporated acid, thereby releasing the protons within the surface layer. The strong underlying continuum within the surface spectrum appears consistent with a significant extent of proton delocalization within the surface. Note that the proton delocalization takes place here in a solid experimental system. (The cluster models are also solid, in the sense that heavy atoms do not exchange places on the time scale of the simulation.)

A related spectral pattern was measured for the mixed amorphous 1:4 solid, with broad bands and underlying continuum. The spectrum thus suggests similar delocalization within this solid phase. One can envisage a solid structure dominated by mixed chains of methanol and HCl molecules. Some of the acid acquires a third hydrogen bond, ionizes, and releases a proton into the chain. However in methanol-rich solids, the third bond is likely to be supplied by methanol (say, at a "head" position of a neighboring chain) rather than by HCl. A ring cluster shown in Figure 6g constitutes a crude model for this physical behavior. A ring cluster with four methanol molecules and an HCl is solvated by an additional methanol molecule bonded at the chloride position. The cluster displays, in fact, proton delocalization over all methanol positions within the ring, and moreover, its spectrum is similar to that of the 1:4 solid (compare spectra in Figure 1 panels C and H). (Excess absorption at $\sim$1000 cm^{-1} in the experimental spectrum suggests that some acid remains doubly coordinated in a proton-sharing configuration.)

Finally, preliminary results are reported on the spectrum of the acid-rich amorphous 1:1 HCl/methanol phase. The solid appears to be mostly ionic, in analogy to the amorphous 1:1 HCl monohydrate. The measured spectrum is in agreement with the one calculated for the alternating acid-methanol-acid-methanol ring cluster. The cluster is fully ionic and is composed of alternating methoxonium and chloride units (Figure 6h). In this case, the ionization is induced by mutual solvation of the components. Here, the protons are localized on methoxonium units, rather than fluxional, as also evidenced by the absence of an underlying continuum in the calculated spectrum (Figure 1J). A modest continuum contribution to the measured spectrum in Figure 1E reflects most likely some contribution of proton-sharing configurations in the amorphous solid; this contribution is reduced in the related 1:1 crystals.[25] (A detailed study of mixed crystalline and amorphous acid/methanol solids will be published separately.)

In the long run, the mixed HCl/methanol systems of our interest should and will be studied by use of more realistic condensed-phase models. However, already at the present level of modeling, employing small clusters, the calculations confirm the strengths of on-the-fly dynamics in the interpretation of infrared spectra of fluxional systems (see, for example, refs 31, 34, and 50). In contrast to ab initio normal-mode analysis, spectral calculations employing on-the-fly dipole−dipole correlation functions can reproduce broad bands and underlying continua resulting from totally anharmonic proton dynamics. Moreover, in contrast to studies employing empirical potentials, all possible solvation states are included, and parametrization of the potential and of the dipole functions is not needed. The obvious price of the above advantages is a limitation on the system size, the duration of trajectories, and the level of electronic structure calculations, that are feasible in on-the-fly simulations. Nevertheless, the results seem informative and encouraging.

Acknowledgment. The support of the U.S. National Science Foundation and the Israel Science Foundation is gratefully acknowledged. J.S. thanks ICM in Warsaw University for computer time.

Supporting Information Available: Ab initio result summary that gives complete list of energies, bond distances. and frequencies of clusters used in on-the-fly molecular dynamics simulations as well as transition state for cluster shown in Figure 6e and different minima for clusters given in Figure 6e.,f. This material is available free of charge via the Internet at http://pubs.acs.org.

References and Notes

(1) Molina, M. J.; Tso, T. L.; Molina, L. T.; Whang, F. C. Y. *Science* **1987**, *238*, 1253.
(2) Tolbert, M. A.; Rossi, M. J.; Malhotra, R.; Golden, D. M. *Science* **1987**, *238*, 1258.
(3) Devlin, J. P.; Uras, N.; Sadlej, J.; Buch, V. *Nature* **2002,** *417*, 269.
(4) Buch, V.; Sadlej, J.; Aytemiz-Uras, N.; Devlin, J. P. *J. Phys. Chem. A* **2002**, *106*, 9374.
(5) Kang, H.; Shin, T. H.; Park, S. C.; Kim, I. K.; Han, S. J. *J. Am. Chem. Soc.* **2000**, *122*, 9842.
(6) Haq, S.; Harnett, J.; Hodgson, A. *J. Phys. Chem. B* **2002**, *106*, 3950.
(7) Isakson, M. J.; Sitz, G. O. *J. Phys. Chem. A* **1999**, *103*, 2044.
(8) Andersson, P. U.; Nagard, M. B.; Pettersson, J. B. C. *J. Phys. Chem. A* **2000**, *104*, 1596.
(9) Svanberg, M.; Pettersson, J. B. C.; Bolton, K. J. *J. Phys. Chem. A* **2000**, *104*, 5787.
(10) Al-Halabi, A.; Kley, A. W.; Kroes, G. J. *Chem. Phys. Lett.* **1999**, *307*, 505.
(11) Kroes, G. J.; Clary, D. C. *J. Phys. Chem.* **1992**, *96*, 7079.
(12) Clary, D. C.; Wang, L. *J. Chem. Soc., Faraday Trans.* **1997**, *93*, 2763.
(13) Devlin, J. P., Farni, M.; Suhm, M. A.; Buch, V. *J. Phys. Chem. A* **2005**, *109*, 955.
(14) Zundel, G. *Adv. Chem. Phys.* **2000**, *111*, 1.
(15) Whalley, E.; Falk, M., *J. Chem. Phys.* **1961**, *34*, 1554.
(16) Uras-Aytemiz, N.; Sadlej, J.; Devlin, J. P.; Buch, V. *Chem. Phys. Lett.* **2006**, *422*, 179.
(17) Buck, U.; Huisken, F. *Chem. Rev.* **2000**, *100*, 3863.
(18) Hagemeister, F. C.; Gruenloh, C. J.; Zwier, T. S. *J. Phys. Chem. A* **1998**, *102*, 82.
(19) Zakharov, V. V.; Brodskaya, E. N.; Laaksonen, A. *J. Chem. Phys.* **1998**, *109*, 9487.
(20) Cope, P.; Legon, A. C.; Millen, D. J. *Chem. Phys. Lett.* **1984**, *112*, 59.
(21) Tan, X.-Q.; Ioannou, I. I.; Kuczkowski, R. L. *J. Mol. Struct.* **1995**, *356*, 105.
(22) Fárník, M.; Weimann, M.; Suhm, M. A. *J. Chem. Phys.* **2003**, *118*, 10120.
(23) Weimann, M.; Fárník, M.; Suhm, M. A.; Alikhani, M. E.; Sadlej, J. *J. Mol. Struct.* **2006**, *790*, 18.
(24) Andrzejewska, A.; Sadlej, J. *Chem. Phys. Lett.* **2004**, *393*, 228.
(25) Devlin, J. P.; Sadlej, J.; Hollman, M.; Buch, V. *J. Phys. Chem. A* **2004**, *108*, 2030.
(26) Morrone, J. A.; Tuckerman, M. E. *J. Chem. Phys.* **2002**, *117*, 4403.
(27) Chang, H.-C.; Jiang, J.-C.; Chang, H.-C.; Wang, L. R.; Lee, Y. T. *Isr. J. Chem.* **1999**, *39*, 231.
(28) Chang, H.-C.; Jiang, J.-C.; Lin, S. H.; Lee, Y. T.; Chang, H.-C. *J. Phys. Chem. A* **1999**, *103*, 2941.
(29) Fujii, A.; Enomoto, S.; Miyazaki, M.; Mikami, N. *J. Phys. Chem. A* **2005**, *109*, 138.
(30) Solca N.; Dopfer O. *J. Phys. Chem. A* **2005**, *109*, 6174.
(31) Buch, V.; Mohamed, F.; Krack, M.; Sadlej, J.; Devlin, J. P.; Parrinello, M. *J. Chem. Phys*. **2004**, *121*, 12135.
(32) VandeVondele, J.; Krack, M.; Mohamed, F.; Parrinello, M.; Chassaing, T.; Hutter, J. *Comput. Phys. Commun.* **2005**, *167*, 103.
(33) CP2K, http://cp2k.berlios.de (2000−2004).
(34) Iyengar, S. S.; Petersen, M. K.; Day, T. J. F.; Burnham, C. J.; Teige, V. E.; Voth, G. A. *J. Chem. Phys.* **2005**, *123*, 084309.

(35) Buch, V.; Bauerecker, S.; Devlin, J. P.; Buck, U.; Kazimirski, J. K. *Int. Rev. Phys. Chem.* **2004**, *23*, 375.
(36) Parent, Ph.; Laffon, C. *J. Phys. Chem. B* **2005**, *109*, 1547.
(37) Goedecker, S.; Teter, M.; Hutter, J. *Phys. Rev. B* **1996**, *54*, 1703.
(38) Becke, A. D. *Phys. Rev. A* **1998**, *38*, 3098.
(39) Lee, C. T.; Yang, W. T.; Parr, R. G. *Phys. Rev. B* **1988**, *37*, 785.
(40) Frisch, M. J., et al. Gaussian 98, Revision A.7; Gaussian, Inc.: Pittsburgh, PA, 1998.
(41) Smith, A.; Vincent, M. A.; Hiller, I. H. *J. Phys. Chem. A* **1999**, *103*, 1132.
(42) Bacelo, D. E.; Binning, R. C.; Ishikawa, Y. *J. Phys. Chem. A* **1999**, *103*, 4631.
(43) (a) Xantheas S. S.; Dunning, T. H. *J. Chem. Phys.* **1993**, *99*, 8774. (b) Xantheas S. S. *J. Chem. Phys.* **1994**, *100*, 7523.
(44) Huber, K. P.; Herzberg, G. *Molecular Spectra and Molecular Structure IV, Constants of Diatomic Molecules*; Van Nostrand Reinhold: New York, 1979.
(45) Harmony, M. D.; Laurie, V. W.; Kuczkowski, R. L.; Schwendeman, R. H.; Ramsay, D. A.; Lovas, F. J.; Lafferty, W. J.; Maki, A. G. *J. Phys. Chem. Ref. Data* **1979**, *8*, 619.
(46) Chaban, G. M.; Gerber, B. R.; Janda, K. C. *Phys. Chem. A* **2001**, *105*, 8323.
(47) Agmon, N. *Chem. Phys. Lett.* **1995**, *244*, 456.
(48) Ando, K.; Hynes, J. T. *J. Phys. Chem. B* **1997**, *101*, 10464.
(49) Yoon, Y. K.; Carpenter, G. B. *Acta Crystallogr.* **1959**, *12*, 17.
(50) Gaigeot, M. P.; Vuilleumier, R.; Sprik, M.; Borgis, D. *J. Chem. Theor. Comput.* **2005**, *1*, 772.